Title

Facile integration of low-cost black phosphorus in solution-processed organic solar cells with improved fill factor and device efficiency

Authors

Zhao, Yun
Chen, Teresa L
Xiao, Liangang
et al.

Publication Date

2018-11-01

DOI

10.1016/j.nanoen.2018.08.063

Peer reviewed

Facile Integration of Low-Cost Black Phosphorus in Solution-Processed Organic Solar Cells with Improved Fill Factor and Device Efficiency

Yun Zhao[a,b]*, Teresa L. Chen[a], Liangang Xiao[a,c], Matthew A. Kolaczkowski[a,d], Liang Zhang[e], Liana M. Klivansky[a], Virginia Altoe[a], Bining Tian[f], Jinghua Guo[e], Xiaobin Peng[c], Yue Tian[f]*, Yi Liu[a]*

[a]The Molecular Foundry, Lawrence Berkeley National Laboratory, Berkeley, California 94720, United States
[b]School of Chemical Engineering and Technology, China University of Mining and Technology Xuzhou 221116, China
[c]Institute of Polymer Optoelectronic Materials and Devices, State Key Laboratory of Luminescent Materials and Devices, South China University of Technology, 381 Wushan Road, Guangzhou 510640, P.R. China
[d]Department of Chemistry, University of California, Berkeley, Berkeley, California 94720, United States
[e]Advanced Light Source, Lawrence Berkeley National Laboratory, Berkeley, California 94720, United States
[f]Key Lab of Advanced Transducers and Intelligent Control System of Ministry of Education, College of Physics and Optoelectronics, Taiyuan University of Technology, Taiyuan 030024, China

yliu@lbl.gov
zhaoyun@cumt.edu.cn
tianyue@tyut.edu.cn

Abstract

Black phosphorus (BP) as a promising two-dimensional (2D) material has gained great attention in nanoelectronic devices because of its intrinsic semiconductor characteristics. However, the poor material availability and solution processability have been major roadblocks that hinder its wider application in microelectronics. Herein, readily available, lost-cost BP was utilized as an effective component that was integrated via a facile solution process for the fabrication of bulk heterojunction organic solar cells (OSCs). An impressive fill factor (FF) of 74.2% and power conversion efficiency (PCE) of 10.5% were realized in the OSCs incorporating 10wt% of BP in the active layer of the benchmark polymer donor PTB7-Th and PC71BM acceptor,

corresponding to a 20% PCE enhancement compared to the BP-free binary devices. The efficiency enhancement can be attributed to BP's high hole carrier mobility that facilitates better carrier extraction and suppression of the recombination. BP has been further demonstrated to be effective in additional solar cells based on other photovoltaic (PV) materials, including non-fullerene OSCs. The successful incorporation of the inexpensive BP in the solution-based fabrication of OSCs opens the door for its application in high performance, low cost flexible electronics.

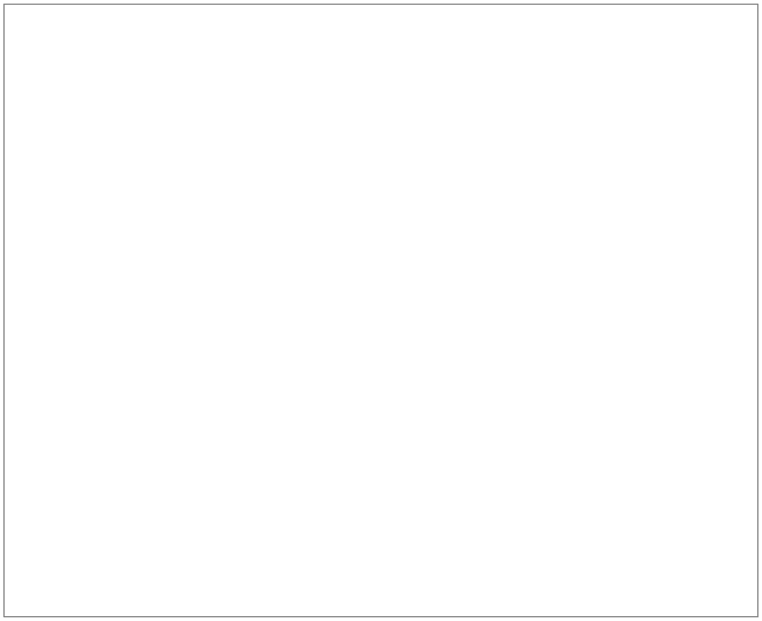

Keywords: black phosphorus, fill factor, hole transport, organic solar cell, solution processability

1. Introduction

As a potential alternative to silicon-based solar cell, bulk heterojunction (BHJ) organic solar cells (OSCs) feature advantages such as low cost, light weight, mechanical flexibility, and amenability to manufacturing by high-throughput and large-area roll-to-roll coating processes [1-5]. To date, power conversion efficiency (PCE) of OSCs higher than 14% has been achieved

through the combined development of high-performance materials [6-8], better morphology control [9-10], and new device architectures [11-13]. However, the relatively low carrier mobility of organic semiconductors limits the charge collection efficiency and still remains to be a great challenge for improving the efficiency of OSCs. The thickness of active layers of OSCs is usually limited to approximately 100 nm to ensure efficient charge transport, which restricts the absorption. Many approaches have been implemented to improve charge carrier mobilities, including thermal annealing [14-15], solvent annealing [16-17], the use of additives [18-19] and the ternary components [20-21]. Such approaches may lead to decreased series resistances (R_s) and/or increased shunt resistance (R_{sh}), which contribute to enhanced short circuit current (J_{SC}), open-circuit voltage (V_{OC}), fill factor (FF), and the overall PCE.

Recently, black phosphorus (BP), an allotrope of phosphorus with a two-dimensional (2D) layered structure, has received great attention because of its intrinsic semiconductor characteristics and high charge carrier mobilities [22-~~24~~25]. The bandgap of BP can be modulated from 0.3 eV for the bulk to 1.8 eV for bilayers and further to 2.1 eV for the monolayer. Few-layered BP exhibits high mobility of up to ~1000 $cm^2V^{-1}s^{-1}$ in field-effect transistors [~~25~~26]. The superior semiconducting properties of BP have generated considerable interests for its application in OSCs to overcome the charge mobility limitation. For example, efficient hetero-junction solar cells using BP and PC61BM (PC61BM: [6,6]-phenyl-C61-butyric acid methyl ester) as active materials were reported by Zhao and coworkers [~~26~~27]. BP in the form of quantum dots (QDs) was utilized by Yan and coworkers for improving light harvesting in OSCs at 0.055wt% loading [~~27~~28]. BP QDs were also reported as charge transport layer in OSCs [~~28~~29], dye sensitized solar cells [~~29~~30] and perovskite solar cells [~~30~~31]. Despite these demonstrated advances, BP's application in photoelectric devices is greatly restricted, largely due

to its limited processability and stability. Exfoliation from BP single crystals is the dominant method to prepare few-layer BP samples, which is a low throughput and cost ineffective process [23]. The scale and scope of BP's application in OSCs is also limited by its solution processability, as BP clusters have poor dispersibility in organic solvents and are mainly processed in the form of nanoparticles [~~31~~32]. As a result, the loading of BP in the active layer of OSCs is greatly limited.

We have shown recently that a solution-based method has been developed to produce BP in multi-gram quantity from cheap and readily available white phosphorus via a one-step solvothermal method [~~32~~33-~~33~~34]. The thus obtained BP also exhibits high air stability due to its partially oxidized nature. Despite their demonstrated catalytic activity for photo-driven water splitting, its full potential for optoelectronics such as OSCs has remained unexplored. Herein, we take advantage of the facile, scalable and low-cost synthesis of BP (less than $1 per gram) by using it as a charge-transport mediator in BHJ OSCs. Good dispersity of BP in organic solvent is achieved when being processed together with the donor polymer, poly[4,8-bis(5-(2-ethylhexyl)thiophen-2-yl)benzo[1,2-b;4,5-b']dithiophene-2,6-diyl-alt-(4-(2-ethylhexyl)-3-fluorothieno[3,4-b]thiophene-)-2-carboxylate-2-6-diyl)] (PTB7-Th) (**Fig. 1**a). Together with [6,6]-phenyl-C71-butyric acid methyl ester (PC71BM) as the acceptor, high performance OSCs have been realized, which show an improved FF of 74.2% and around 20% PCE enhancement compared to the BP-free binary devices. To the best of our knowledge, this is the highest performance OSC can be achieved utilizing a high loading of BP in the active layer.

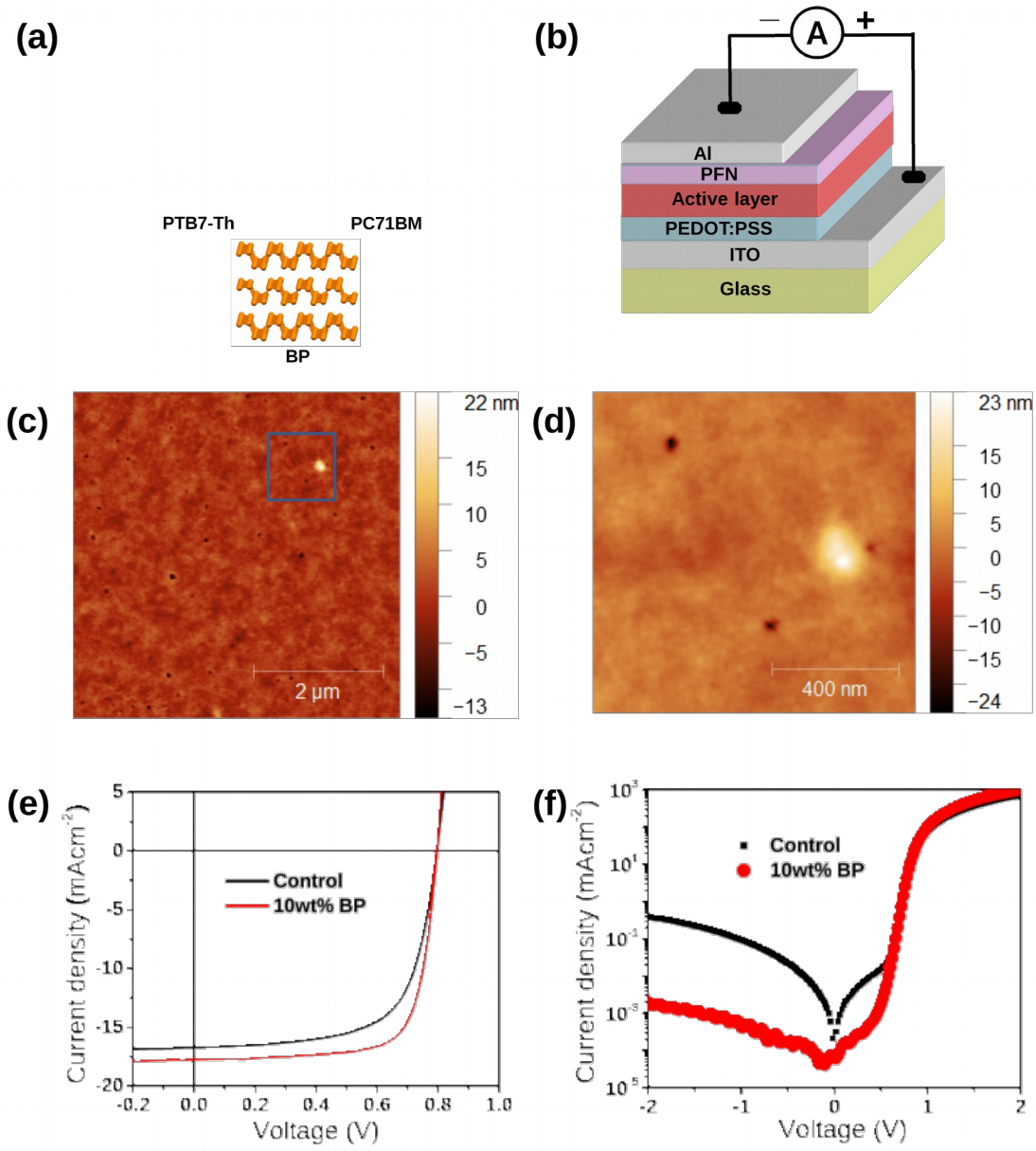

Fig. 1. (a) Molecular structures of PTB7-Th and PC71BM, and the layered structure of BP. (b) Device architecture of the OSC. (c) AFM height images for PTB7-Th:PC71BM:BP ternary film, and (d) the blowup of the area indicated by the blue square in (c). (Photovoltaic) PV performance of the control PTB7-Th:PC71BM OSC without BP (black) and the OSC with 10wt% BP loading (red): (e) current density-voltage (J-V) curves under the illumination of AM 1.5G, 100 $mWcm^{-2}$; (f) dark currents of the OSCs.

2. Results and discussion

We first investigated whether BP is compatible with the solution-based device fabrication process. The thickness of the as-synthesized BP is in the range of 1–15 nm ~~The BP used here was as-synthesized with the thickness ranging from 1-15 nm~~ [33]. A mixture of active materials and 10wt% BP was dispersed in chlorobenzene and stirred overnight. Then the mixture was filtered through a syringe filter with pore size of 1 μm to remove large BP aggregates. The presence of the donor polymer is critical as it helps to disperse BP into smaller particles and sieve through the filter, from which continuous thin films could be obtained by spincasting. In the absence of PTB7-Th, very little BP remains in the filtrate from a BP-only or BP/PCBM dispersion. Presumably, the noncovalent interactions between PTB7-Th and BP facilitates the BP sheets exfoliation and in turn forms a better dispersion. Scanning electron microscope (SEM) and atomic force microscope (AFM) measurements were carried out to study the morphologies of these blend films and to verify the presence of BP. SEM images of the ternary film reveal particles on the film surface with approximate sizes of 200 nm (Fig. S1b and S1c in the Supporting Information, SI), which are absent in the BP-free thin films (Fig. S1a in the SI). The elemental mapping of these surface particles clearly indicates the presence of phosphorus (Fig. S1d in the SI), confirming their identity as BP clusters. The presence of BP clusters on the surface of thin films is also confirmed by AFM studies (Fig. 1c and 1d). In addition, holes with a width of ~50 nm and a depth of 10-20 nm (Fig. 1c-d and S2c-d in the SI) are observed to distribute across the surface of the PTB7-Th:PC71BM:BP ternary blend film, the formation of which is attributed to the precipitation of BP clusters to the bottom of the active layer during the spin-coating process. These holes are distinct from the shallow voids formed in the BP-free binary mixture (Fig. S2a-b in the SI). ~~These~~ Such results suggest that BP exist in the form of

small particles and are dispersed across the active layer ~~.~~ with the lateral size estimated to be 50-200 nm. ~~and the size of BP can be estimated to 50-200 nm.~~ The root-mean-square (RMS) roughness of the ternary blend film (1.743 nm) increases only slightly compared with the binary blend film (RMS=1.310 nm), indicating that the majority of BP is blended into the matrix of the active layer without significant change of the surface roughness. Spuncast films were also prepared from unfiltered samples, where large BP aggregates with sizes over 1 μm were clearly observed from the SEM image (Fig. S3 in the SI). As shown in later sections, the surface BP clusters neither interfere with solar cell device fabrication nor dramatically degrade the device performance.

With successful incorporation of BP into the spuncast active layer, OSCs were fabricated using the conventional device structure of indium tin oxide (ITO)/poly(3,4-ethylenedioxythiophene):poly(styrene sulfonate) (PEDOT:PSS)/active layer/PFN/Al, where poly[(9,9-bis(3'-(N,N-dimethylamino)propyl)-2,7-fluorene)-alt-2,7-(9,9-dioctylfluorene)] (PFN) was used as the cathode interfacial layer [~~34~~35]. None of the binary solar cells using the blends of PTB7-Th:BP or BP:PC71BM show PV responses, indicating that BP alone is not a suitable acceptor (A) or donor (D) material. BP was thus primarily used as a third component for the fabrication of ternary solar cells while keeping the weight ratio of PTB7-Th:PC71BM at 1:1.5. PV performance of the PTB7-Th:PC71BM:BP blend at various BP loading and thickness under the illumination of AM 1.5 G, 100 $mWcm^{-2}$ are summarized in **Table 1**.

Table 1. PV performance of the PTB7-Th:PC71BM:BP blend at various BP loading and thickness of the active layer. Statistical data were based on 10 devices.

BP loading[a)]	Thickness	V_{OC}	J_{SC}	FF	PCE	PCE_{best}

(wt%)	(nm)	(V)	($mAcm^{-2}$)	(%)	(%)	(%)
0	100	0.785±0.005	16.5±0.1	69.4±0.7	9.0±0.1	9.08
10	100	0.795±0.005	16.5±0.1	72.7±1.1	9.6±0.3	9.86
0	150	0.795±0.005	16.7±0.2	66.4±0.9	8.6±0.2	8.81
3	150	0.795±0.005	16.7±0.2	72.5±1.0	9.5±0.2	9.73
7	150	0.795±0.005	16.8±0.2	72.9±1.0	9.6±0.2	9.76
10	150	0.795±0.005	17.8±0.2	73.4±1.1	10.3±0.2	10.5
13	150	0.795±0.005	17.6±0.2	73.1±1.1	10.1±0.3	10.4
16	150	0.795±0.005	17.1±0.2	72.6±1.0	9.7±0.3	10.0
0	200	0.785±0.005	17.2±0.3	62.9±0.7	8.4±0.2	8.59
10	200	0.795±0.005	18.2±0.3	66.2±1.3	9.5±0.2	9.65

[a)]The wt% is the composition of BP in the unfiltered mixture.

The binary PTB7-Th:PC71BM device with a 100 nm-thick active layer exhibits a V_{OC} of 0.785 V, a J_{SC} of 16.5 mA cm^{-2} and a FF up to 70.1%. The maximum PCE for this cell is 9.08%, similar to the literature reports [~~35~~36-~~36~~37]. When increasing the thickness of the active layer, the FF decreases to about 66.4% for the 150 nm-thick devices and further to around 62.9% for the 200 nm-thick ones, consistent with the higher recombination loss of free carriers due to the low carrier mobility of organic materials [~~37~~38-~~38~~39]. In comparison, after incorporation of BP, the FF is increased at all thicknesses. As shown in Table 1, the V_{OC} remains identical at around 0.79 V and is independent of the addition of BP and the film thickness. Slight J_{SC} increase is observed for 150 nm and 200 nm thick films. The most significant increase is FF, which increases to up to 74.2% for 150 nm-thick devices, amounting to an optimal PCE of 10.5% with 10wt% BP loading. Remarkably, devices fabricated without filtering off the large clusters of BP still show very good device performances despite the very rough surface of active layers (Fig. S4

in the SI). As shown in Table S1 in the SI, unfiltered BP-containing devices at active layer thicknesses of 150 nm and 200 nm exhibit PCEs of 10.0% and 9.64%, respectively, all outperforming the BP-free control devices.

Fig. 1(e) compares the J-V behavior of the binary and ternary OSCs with 10wt% BP loading at a thickness of 150 nm. The corresponding external quantum efficiency (EQE) spectra are shown in Fig. S5 in the SI. The parameters of the best binary solar cells at this thickness are as the following: V_{OC}=0.795 V, J_{SC}=16.7 mAcm^{-2}, FF=66.4% and PCE=8.81%. In the ternary system that involves 10wt% BP, the J_{SC} is increased slightly to 17.8 mAcm^{-2}, while the FF undergoes a significant increase to 74.2%, leading to a PCE of 10.5% and around 20% enhancement compared to the control binary device. UV/Vis absorption spectra of PTB7-Th:PC71BM binary films and PTB7-Th:PC71BM:BP ternary films are very similar, suggesting that BP has negligible contribution to the overall thin film absorption (Fig. S6 in the SI). As a result, the slight increase of EQE value and the corresponding J_{SC} can be attributed to more efficient charge collection due to the addition of BP.~~As a result, the slightly increase of EQE value and the corresponding J_{SC} can be attributed to more collected charges.~~ From the dark currents of the solar cells (Fig. 1f), it is found that the rectification ratio of BP-based device is increased by two order of magnitudes, together with an increase of R_{sh} from 6.1×10^{4} to 1.1×10^{6} Ωcm^{-2} and a decrease of R_s from 1.4 to 1.0 Ωcm^{-2}. The better overall diode characteristics suggests that the BP-containing OSCs have lower recombination of free carriers and better efficiency of carrier extraction [~~39~~40-~~40~~41], corroborating with enhanced FF and overall PCE.

Grazing incidence X-ray diffraction (GIXD) was carried out to probe the crystallinity and molecular packing behavior in the binary and ternary thin films. As shown by the 2D GIXD patterns and corresponding line-cuts in **Fig. 2**, both the binary and ternary system show similar

diffraction patterns and intensities that correspond to the coexistence of face-on oriented PTB7-Th crystallites and randomly oriented PC71BM crystallites. The nearly identical morphologies suggest that the presence of BP has little effect on the donor-acceptor crystallization and nanoscale phase separation. This is further confirmed by resonant soft X-ray scattering (RSoXS) studies, which reveal that the characteristic length scale of nanoscale phase separation is around 40 nm for both binary and ternary films (Fig. S7 in the SI).

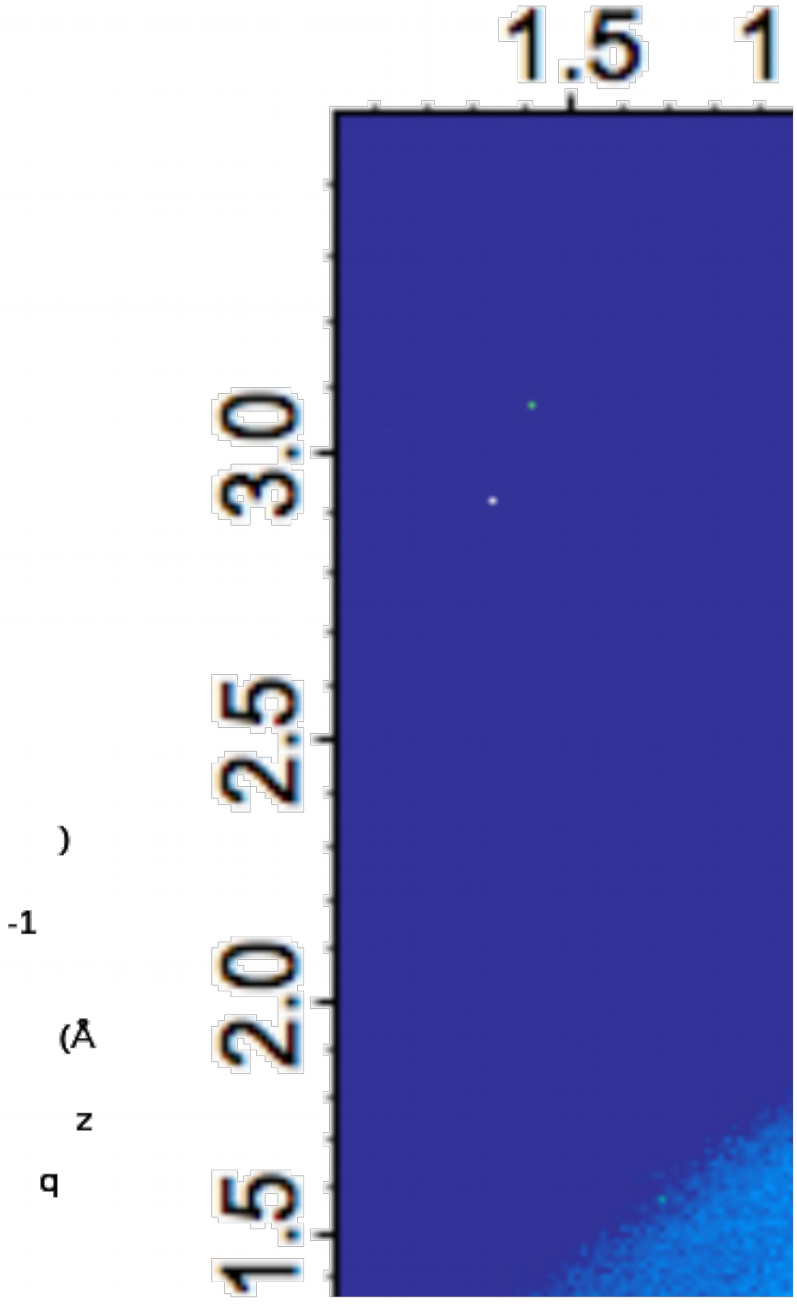

Fig. 2. 2D GIWAXS patterns of PTB7-Th:PC71BM:BP thin films at various BP loading: (a) 0wt % (control), (b) 3wt%, (c) 7wt%, (d) 10wt%. (e) and (f) are vertical and horizontal linecuts of these scattering profiles.

Single carrier devices were fabricated to understand the impact of BP on the charge transport behavior of the active materials. The hole-only devices were fabricated using the structure of ITO/PEDOT:PSS/active layer/MoO_3/Al (**Fig. 3**a) and for the electron-only devices, a device structure of ITO/ZnO/active layer/Al was used (Fig. 3b). All the single carrier ~~hole and electron~~ devices were tested ~~at~~in the dark. The J-V curves of the devices based on BP-free binary mixtures are more symmetric under positive and negative bias for both hole-only and electron-only devices. When BP is incorporated, both ternary devices exhibit a more rectified diode response. Notably, the BP-containing hole-only device shows an increased current density at the same negative voltage than the BP-free device (Fig. 3a), corresponding to a hole mobility (μ_h, measured using the space-charge limited current (SCLC) method) enhancement from 6.4×10^{-4} $cm^2V^{-1}s^{-1}$ to around 1.3×10^{-3} $cm^2V^{-1}s^{-1}$ after the incorporation of BP. The μ_h of ternary PTB7-Th:PCBM devices at different BP loadings were also measured. As shown in Fig. 3c and S8 in the SI, μ_h increases in all the ternary blends, which shows excellent correlation with the dependence of FF on BP loading (Fig. 3d) [~~41~~42-~~42~~43]. These results strongly support a BP-assisted hole transport in the active layers. As measured by ultraviolet photoelectron spectroscopy (UPS) (Fig. S9 in the SI), the valence band (VB) of BP is -5.3 eV, which matches well with the highest occupied molecular orbital (HOMO) level of PTB7-Th (-5.2 eV). Hole transfer between PTB7-Th and BP was supported by Carbon K-edge X-ray absorption spectroscopy (XAS) and X-ray emission spectroscopy (XES) measurements. Fig. S10a and S10b in the SI shows the C K-edge XES and XAS of the pristine PTB7-Th and its blend with BP and the corresponding first derivative data. The absorption feature of PTB7-Th, which reflects the local density of unoccupied electronic states, shifts to the lower energy level, indicating the occurrence of hole transfer from PTB7-Th to BP [~~43~~44]. On the other hand, the more apparent

rectification in BP-containing devices suggests that the hole injection barrier near the PEDOT side is larger than the MoO_3 side. A sketch of the corresponding energy diagram is shown in the inset of Fig. 3a.

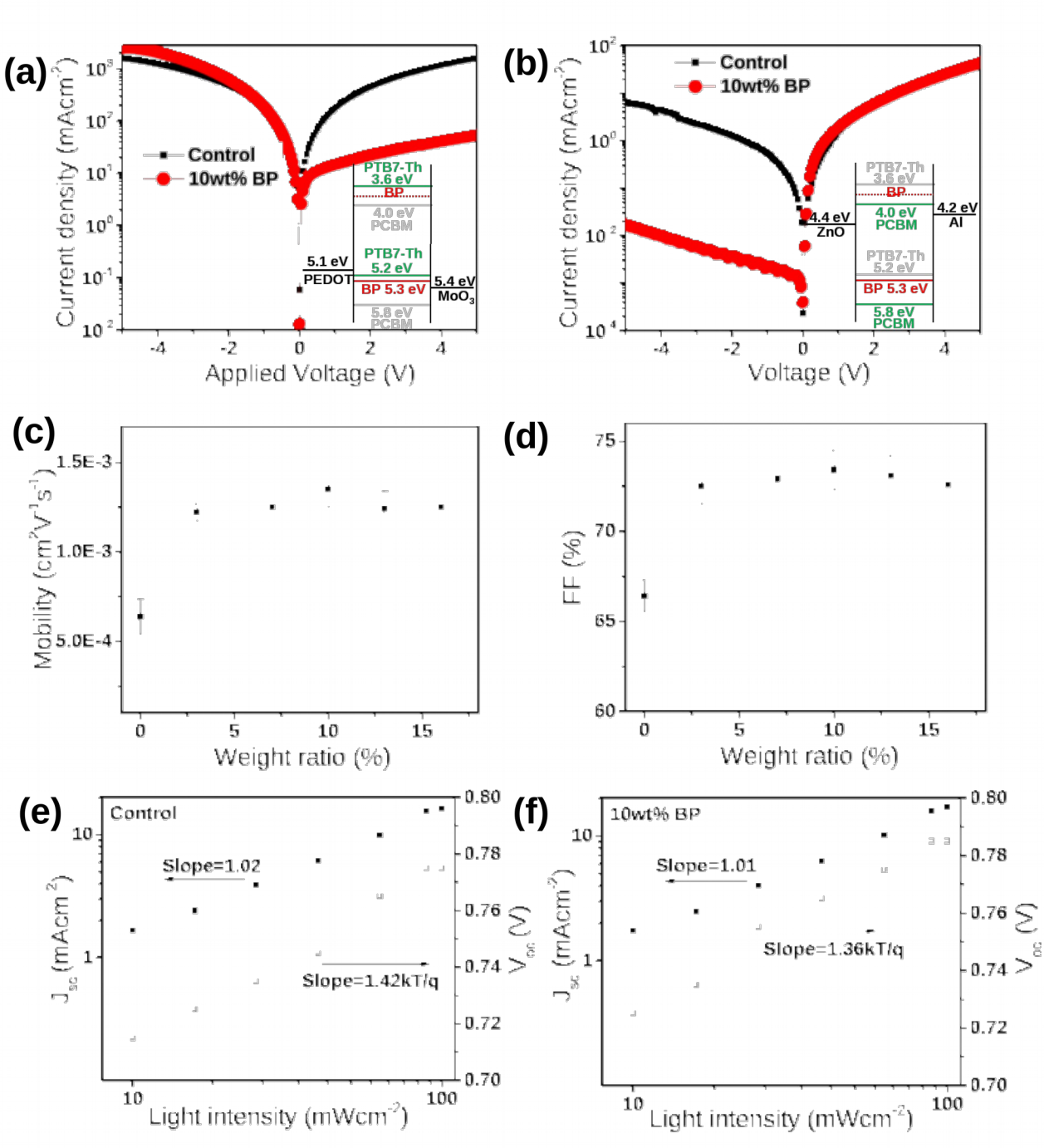

Fig. 3. (a) J-V curves obtained for hole-only and (b) electron-only devices based on control PTB7-Th:PC71BM blend film without BP (black) and with 10wt% BP loading (red). The insets show the energy diagrams of devices. (c) The plots of hole mobility and (d) FF of the PTB7-Th:PCBM devices at various BP loading. The thickness of active layer was kept at 150 nm. (e) Plots of J_{SC} and V_{OC} of the control PTB7-Th:PC71BM OSC and (f) the OSC with 10wt% BP loading at different light intensities.

The conduction band (CB) of BP is not able to be directly measured but estimated to be between the lowest unoccupied molecular orbital (LUMO) levels of PTB7-Th (-3.6 eV) and PC71BM (-4.0 eV) based on the electron transporting behavior of the electron-only devices. For the electron-only devices, the BP-containing ones show a similar current density to that of the binary device at positive bias but a much lower current density at negative bias (Fig. 3b). This rectified diode response indicates that BP creates an electron injection barrier greater than 0.4 eV, a barrier defined by the energy difference between the CB of ZnO (-4.4 eV) and LUMO of PC71BM (-4.0 eV). It can thus be inferred that the CB of BP is higher than -4.0 eV. On the other hand, the CB of BP should be lower than the LUMO of PTB7-Th (-3.6 eV) considering the similar current densities on the positive scan for the binary and ternary devices. An energy diagram correlating to the electron-transporting diode is illustrated in the inset of Fig. 3b. Furthermore, the similar current density at positive bias indicates little improvement of electron mobility after BP incorporation, which may be attributed to the relatively misaligned energy levels as well as the weak interactions between PC71BM and BP.~~Furthermore, the similar current density at positive bias indicating unchanged electron mobility of active layer after integrating with BP, which can be attributed to the constant crystallization and nanoscale phase size of PC71BM discussed above.~~

To further understand the role of BP in the ternary system, the recombination mechanism for the binary and ternary OSCs with 10wt% BP loading was investigated by measuring J_{SC} and V_{OC} as a function of light intensity. As shown in Fig. 3e and 3f, the slopes of the double-logarithmic plots of J_{SC}-light intensity for the binary and ternary devices are 1.02 and 1.01, respectively, suggesting similar low levels of bimolecular recombination in both devices. Under open-circuit conditions, the dependence of V_{OC} on the logarithm of the light intensity is related to the recombination mechanism. Bimolecular recombination has a slope of *kT/q*, while trap-assisted recombination has a slope of 2 *kT/q*. As can be seen from Fig.s 3e and 3f, the slopes of the device decreases from 1.42 *kT/q* to 1.36 *kT/q* after incorporation of BP, which indicates suppression of trap-assisted recombination [~~44~~45-~~45~~46]. The above studies collectively suggest that in the PTB7-Th:PC71BM:BP ternary blend, BP efficiently extracts the hole from the donor-acceptor interface and transfers it to the anode, resulting in suppressed carrier recombination and enhanced FF. Furthermore, the unprecedented roughness tolerance in OPVs correlates strongly with BP's superior charge transporting capability that can compensate the recombination loss and other losses incurred by the inferior film morphology.

Encouraged by the successful improvement of PV performance of PTB7-Th:PC71BM based devices, we have incorporated BP at 10wt% loading into additional devices using different PV material systems, which include the donor/acceptor pairs based on J71/ITIC and J71/PC71BM (**Fig. 4**). As shown in Fig. 4b and 4c and **Table 2**, the introduction of BP results in increased FF and PCEs in all cases. Notably, the non-fullerene solar cells based on J71:ITIC were fabricated at both as-cast (Table 2) and thermal annealing conditions (Table S2 in SI). Incorporation of BP in non-annealed devices can increase the device efficiency to a similar level of the thermal-treated devices. These positive results are consistent with that observed in the

PTB7-Th:PC71BM system, strongly supporting the general applicability of BP serving as a charge transport mediator to improve device performances, including non-fullerene OSCs.

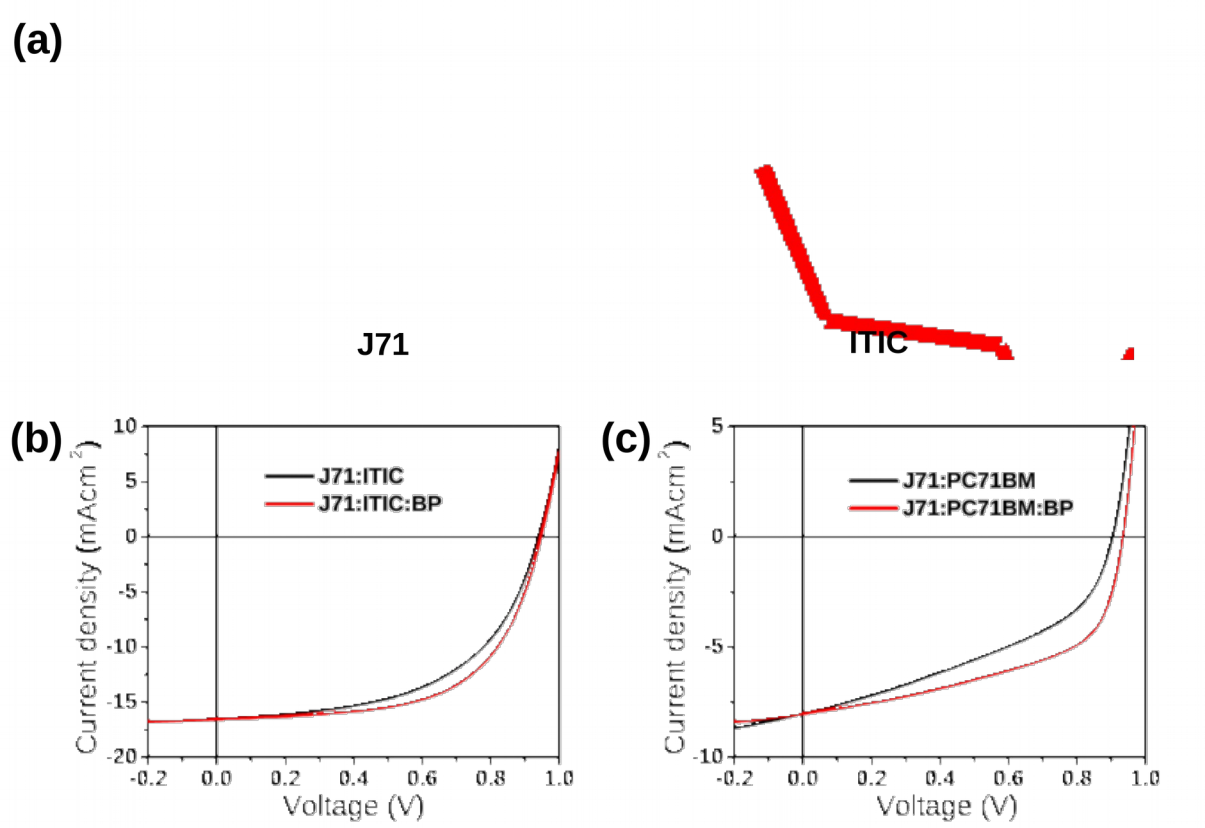

Fig. 4. Molecular structures of (a) J71and ITIC. (b) J-V curves of OSCs based on J7I:ITIC and (c) J71:PC71BM with or without BP under the illumination of AM 1.5G, 100 mWcm^{-2}.

Table 2. PV performance of OSCs based on several different active layers with or without BP under the illumination of AM 1.5G, 100 mWcm^{-2}.

Active layer	V_{OC} (V)	J_{SC} (mAcm^{-2})	FF (%)	PCE (%)
J71:ITIC[a)]	0.935	16.5	54.5	8.41
J71:ITIC:BP [a)]	0.945	16.6	60.0	9.41

J71:PC71BM [b)]	0.905	8.03	41.6	3.02
J71:PC71BM:BP [b)]	0.935	8.06	52.7	3.97

[a)]Fabricated using an inverted device structure of ITO/ZnO/Active layer/MoO_3/Al. [b)]Fabricated using a conventional device structure of ITO/PEDOT:PSS/Active layer/PFN/Al.

3. Conclusion

In summary, low-cost BP prepared in large scale was incorporated for the first time into OSCs as a charge transport mediator for improved PV characteristics. A facile solution processing protocol was developed to incorporate BP into the active layer of PTB7-Th:PC71BM at a loading exceeding previously reported BP-containing OSCs. The BP-containing devices show significantly enhanced device characteristics, with an impressive FF of 74.2% and a PCE of 10.5% at 10wt% BP loading in 150 nm-thick films, corresponding to around 20% PCE enhancement compared with the control binary devices. Detailed morphological and electronic studies illustrate that despite noticeable heterogeneity in the active layer, BP has little impact on the film crystallinity and nanoscale phase separation, yet it can effectively improve hole transport and charge collection. The generality of using BP to improve FF and overall PCE has been demonstrated in additional materials systems, including a non-fullerene OSC. The successful incorporation of BP in OSCs not only provides a cost-effective and robust strategy to improve the performance of OSCs, but also paves the way for the application of BP in flexible organic optoelectronics.

4. Experimental

4.1. Materials

Poly[4,8-bis(5-(2-ethylhexyl)thiophen-2-yl)benzo[1,2-b;4,5-b']dithiophene-2,6-diyl-alt-(4-(2-ethylhexyl)-3-fluorothieno[3,4-b]thiophene-)-2-carboxylate-2-6-diyl)] (PTB7-Th) was purchased from 1 Material, [6,6]-Phenyl-C71-butyric acid methyl ester (PC71BM) was purchased from NanoC, poly [(9,9-bis(3'-(N,N-dimethylamino)propyl)-2,7-fluorene)-alt-2,7-(9,9–dioctylfluorene)] (PFN) was purchased from Derthon Optoelectronic Materials. Black phosphorus (BP) was synthesized according to a previous report [32]. Other materials were purchased from Sigma-Aldrich and used without further purification.

4.2. Device Fabrication and Measurement

The conventional device structure was indium tin oxide (ITO)/ poly(3,4-ethylenedioxythiophene):poly(styrene sulfonate)(PEDOT:PSS)/PTB7-Th:BP:PC71BM/PFN/Al. Prepatterned ITO substrates were cleaned sequentially under sonication in acetone, detergent, deionized water and isopropanol, and then dried at 100 ℃, followed by UV-cleaning for 20 min. The ITO substrates were coated with a 30-nm-thick PEDOT:PSS (Baytron P4083) layer and baked at 120 °C for 20 min. A mixed solution that had a fixed PTB7-Th: PC71BM ratio of 1:1.5 at various BP loading in chlorobenzene (containing 3% v/v of 1, 8-diiodooctane) was spuncast on the PEDOT:PSS layer. The ternary solution was stirred overnight, then filtered through a 1-μm pore size syringe filter to remove the large BP particles. The different thickness of active layer was adjusted by changing the concentration of the solution or the spinning rate. Subsequently, a 5-nm poly[(9,9-bis(3'-(N,N-dimethylamino)propyl)-2,7-fluorene)-alt-2,7-(9,9-dioctylfluorene)] (PFN) layer was spuncast on top of the active layer from methanol solution. Finally, an Al layer of 100-nm thickness was thermally deposited under high vacuum ($\leq 10^{-6}$ mbar) to produce an active area of 0.03 cm^2 for each cell. Hole-only and electron-only devices were fabricated following similar protocols to that of organic solar cells (OSCs)

devices with the structure of ITO/PEDOT:PSS /PTB7-Th:BP: PC71BM/MoO_3/Al and ITO/ZnO /PTB7-Th: BP: PC71BM/Al, respectively. The thickness of the organic and metal layers was determined using a VEECO DEKTAK 150 Stylus profiler. The current density-voltage (J-V) characteristics of the photovoltaic (PV) cells were measured using a computer-controlled Keithley 2400 source meter under AM1.5G illumination from a calibrated solar simulator with irradiation intensity of 100 $mWcm^{-2}$. The external quantum efficiency (EQE) was measured on a commercial Enlitech QE-R measurement system. All fabrications were conducted in a N_2-filled glove box.

4.3. Charge carrier mobility measurement

Charge carrier mobility was measured by space charge limited current (SCLC) method, following the equation $J= (9/8)\varepsilon_0\ \varepsilon_r\mu((V^2)/(d^3))$. Here, J is the current density, μ is the zero-field mobility of holes (μ_h), ε_0 is the permittivity of the vacuum, ε_r is the relative permittivity of the material, d is the thickness of the blend film, and V is the effective voltage ($V = V_{appl}–V_{bi}$, where V_{appl} is the applied voltage to the device, and V_{bi} is the built-in voltage due to relative work function difference of the two electrodes). Here, V_{bi} = 0.1 V for hole-only devices. The mobility was calculated from the slope of $J^{1/2}$-V curves.

4.4. Characterization of GIWAXS and RSoXS

GIWAXS measurements were performed at beamline 7.3.3 of Advanced Light Source (ALS), Lawrence Berkeley National Laboratory (LBNL). Samples were prepared on the Si substrates using identical blend solutions as those used in OSC devices. The 10 keV X-ray beam was incident at a grazing angle of 0.12°-0.16°, selected to maximize the scattering intensity from the samples. The scattered X-rays were detected using a Dectris Pilatus 2M photon counting

detector. Resonant soft X-ray scattering (RSoXS) experiments were performed at beamline 11.0.1.2 of ALS, LBNL. Samples for RSoXS measurements were prepared on a PEDOT:PSS modified Si substrate under the same conditions as used for OSC devices fabrication, and then transferred by floating in water to a Si_3N_4 membrane (1.5mm×1.5mm,100 nm thick) supported by a Si frame (5mm×5mm, 200 μm thick, from Norcada Inc.). 2-D scattering signals were collected in vacuum using a CCD camera (Princeton Instrument PI-MTE).

4.5. Characterization of XAS and XES

The X-ray spectroscopy measurements at the carbon K-edge were performed at the beamline 8.0.1.4 of the ALS, LBNL. Samples were prepared on the Si substrates using the same fabrication conditions as those used in OSC devices. The energy resolution at carbon K-edge was set to 0.1 and 0.3 eV for the XAS and XES measurements, respectively. A highly ordered pyrolytic graphite (HOPG) reference sample was measured before and after the experiments for energy calibration. The XAS spectra were recorded with a defocused beam and the XES spectra were measured with the movement of the samples to mitigate the beam damage effect.

4.6. Other Characterization

The optical absorption of the blend films was measured using a Cary 5000 UV-Vis-NIR spectrometer on quartz substrates. The atomic force microscopy (AFM) measurements were performed on an Asylum MFP-3D Stand Alone AFM from Oxford Instruments. Scanning Electron Microscope (SEM) images were collected on a Zeiss Gemini Ultra-55 Analytical Field Emission Scanning Electron Microscope operated at 5 kV. Valence state of the samples was performed in a Thermo Scientific™ K-Alpha Plus™ X-ray photoelectron spectrometer (XPS) instrument with the capability to acquire Ultraviolet photoelectron spectroscopy (UPS) using He

I ultraviolet light source (21.2eV). The surface of samples was cleaned under a dual monoatomic and gas cluster ion source.

Appendix A. Supporting information

Supplementary data associated with this article can be found in the online version at xxx.

Acknowledgement

This work was performed as user project at the Molecular Foundry, and the X-ray experiments were conducted at the Advanced Light Source (ALS), Lawrence Berkeley National Laboratory, all supported by the Office of Science, Office of Basic Energy Sciences, of the U. S. Department of Energy under Contract No. DE-AC02-05CH11231. Y. Zhao acknowledges the support from Chinese Scholar Counsel.

References

[1] G. Yu, J. Gao, J. C. Hummelen, F. Wudl, A. J. Heeger, Science 270 (1995) 1789.

[2] F. C. Krebs, S. A. Gevorgyan, J. Alstrup, J. Mater. Chem. 19 (2009) 5442.

[3] Y. Zhao, X. Wang, F. Shu, Sol. Energy Mater. Sol. Cells 95 (2011) 684.

[4] L. Lu, T. Zheng, Q. Wu, A. M. Schneider, D. Zhao, L. Yu, Chem. Rev. 115 (2015) 12666.

[5] J. Hou, O. Inganäs, R. H. Friend, F. Gao, Nat. Mater. 17 (2018) 119.

[6] Y. Liang, Y. Wu, D. Feng, S.-T. Tsai, H.-J. Son, G. Li, L. Yu, J. Am. Chem. Soc. 131 (2009) 56.

[7] H. Bin, L. Gao, Z.-G. Zhang, Y. Yang, Y. Zhang, C. Zhang, S. Chen, L. Xue, C. Yang, M. Xiao, Y. Li, Nat. Commun. 7 (2016) 13651.

[8] H. Zhang, H. Yao, J. Hou, J. Zhu, J. Zhang, W. Li, R. Yu, B. Gao, S. Zhang, J. Hou, Adv. Mater., DOI: 10.1002/adma.201800613.

[9] G. Li, V. Shrotriya, J. Huang, Y. Yao, T. Moriarty, K. Emery, Y. Yang, Nat. Mater. 4 (2005) 864.

[10] Y. Huang, E. J. Kramer, A. J. Heeger, G. C. Bazan, Chem. Rev. 114 (2014) 7006.

[11] Z. He, C. Zhong, S. Su, M. Xu, H. Wu, Y. Cao, Nat. Photonics 6 (2012) 591.

[12] A. Tayebeh, K. Parisa, M. Jie, B. C. J., Adv. Mater. 25 (2013) 4245.

[13] X. Zuo, J. Xue, D. Liming, Sci. Bull. 62 (2017) 1562.

[14] W. Ma, C. Yang, X. Gong, K. Lee, A. J. Heeger, Adv. Funct. Mater. 15 (2005) 1617.

[15] Y. Kim, S. Cook, S. M. Tuladhar, S. A. Choulis, J. Nelson, J. R. Durrant, D. D. C. Bradley, M. Giles, I. McCulloch, C.-S. Ha, M. Ree, Nat. Mater. 5 (2006) 197.

[16] Y. Zhao, S. Shao, Z. Xie, Y. Geng, L. Wang, J. Phys. Chem. C 113 (2009) 17235.

[17] G. Zhao, Y. He, Y. Li, Adv. Mater. 22 (2010) 4355.

[18] M. Kim, J. H. Kim, H. Choi Hyun, H. Park Jong, B. Jo Sae, M. Sim, S. Kim Jong, H. Jinnai, D. Park Yeong, K. Cho, Adv. Energy Mater. 4 (2013) 1300612.

[19] J. Zhao, Y. Li, G. Yang, K. Jiang, H. Lin, H. Ade, W. Ma, H. Yan, Nat. Energy 1 (2016) 15027.

[20] H. Huang, L. Yang, B. Sharma, J. Mater. Chem. A 5 (2017) 11501.

[21] P. Cheng, R. Wang, J. Zhu, W. Huang, S. Y. Chang, L. Meng, P. Sun, H. W. Cheng, M. Qin, C. Zhu, X. Zhan, Y. Yang, Adv. Mater. 30 (2018) 1705243.

[22] F. Xia, H. Wang, Y. Jia, Nat. Commun. 5 (2014) 4458.

[23] E. A. Lewis, J. R. Brent, B. Derby, S. J. Haigh, D. J. Lewis, Chem. Commun. 53 (2017) 1445.

[24] S. Lin, Y. Chui, Y. Li, S. P. Lau, FlatChem 2 (2017) 15.

[25] Z. Liu, S. P. Lau, F. Yan, Chem Soc. Rev. 44 (2015) 5638.

[~~25~~26] L. Li, Y. Yu, G. J. Ye, Q. Ge, X. Ou, H. Wu, D. Feng, X. H. Chen, Y. Zhang, Nat. Nanotechnol. 9 (2014) 372.

[~~26~~27] L. Bai, L. Sun, Y. Wang, Z. Liu, Q. Gao, H. Xiang, H. Xie, Y. Zhao, J. Mater. Chem. A 5 (2017) 8280.

[~~27~~28] S. Liu, S. Lin, P. You, C. Surya, P. Lau Shu, F. Yan, Angew. Chem. Int. Ed. 56 (2017) 13717.

[~~28~~29] S. Lin, S. Liu, Z. Yang, Y. Li, W. Ng Tsz, Z. Xu, Q. Bao, J. Hao, C. S. Lee, C. Surya, F. Yan, P. Lau Shu, Adv. Funct. Mater. 26 (2016) 864.

[~~29~~30] Y. Yang, J. Gao, Z. Zhang, S. Xiao, H. H. Xie, Z. B. Sun, J. H. Wang, C. H. Zhou, Y. W. Wang, X. Y. Guo, K. Chu Paul, X. F. Yu, Adv. Mater. 28 (2016) 8937.

[~~30~~31] W. Chen, K. Li, Y. Wang, X. Feng, Z. Liao, Q. Su, X. Lin, Z. He, J. Phys. Chem. Lett. 8 (2017) 591.

[~~31~~32] Y. Zhang, H. Wang, Z. Luo, T. Tan Hui, B. Li, S. Sun, Z. Li, Y. Zong, J. Xu Zhichuan, Y. Yang, A. Khor Khiam, Q. Yan, Adv. Energy Mater. 6 (2016) 1600453.

[~~32~~33] B. Tian, B. Tian, B. Smith, M. C. Scott, Q. Lei, R. Hua, Y. Tian, Y. Liu, Proc. Natl. Acad. Sci. U.S.A 115 (2018) 4345.

[~~33~~34] T. Nilges, Proc. Natl. Acad. Sci. U.S.A 115 (2018) 4311.

[~~34~~35] Z. He, C. Zhong, X. Huang, W. Y. Wong, H. Wu, L. Chen, S. Su, Y. Cao, Adv. Mater. 23 (2011) 4636.

[~~35~~36] S. H. Liao, H. J. Jhuo, Y. S. Cheng, S. A. Chen, Adv. Mater. 25 (2013) 4766.

[~~36~~37] S.-H. Liao, H.-J. Jhuo, P.-N. Yeh, Y.-S. Cheng, Y.-L. Li, Y.-H. Lee, S. Sharma, S.-A. Chen, Sci. Rep. 4 (2014) 6813.

[~~37~~38] S. C. Price, A. C. Stuart, L. Yang, H. Zhou, W. You, J. Am. Chem. Soc. 133 (2011) 4625.

[~~38~~39] G. Zhang, K. Zhang, Q. Yin, X.-F. Jiang, Z. Wang, J. Xin, W. Ma, H. Yan, F. Huang, Y. Cao, J. Am. Chem. Soc. 139 (2017) 2387.

[~~39~~40] Z. E. Ooi, T. L. Tam, A. Sellinger, J. C. deMello, Energy Environ. Sci. 1 (2008) 300.

[~~40~~41] D. S. Leem, A. Edwards, M. Faist, J. Nelson, D. C. Bradley Donal, C. de Mello John, Adv. Mater. 23 (2011) 4371.

[~~41~~42] S. Albrecht, J. R. Tumbleston, S. Janietz, I. Dumsch, S. Allard, U. Scherf, H. Ade, D. Neher, J. Phys. Chem. Lett. 5 (2014) 1131.

[~~42~~43] A. Bartelt Jonathan, D. Lam, M. Burke Timothy, M. Sweetnam Sean, D. McGehee Michael, Adv. Energy Mater. 5 (2015) 1500577.

[~~43~~44] J. A. McLeod, A. L. Pitman, E. Z. Kurmaev, L. D. Finkelstein, I. S. Zhidkov, A. Savva, A. Moewes, J. Chem. Phys. 143 (2015) 224704.

[~~44~~45] Y. J. Kim, C. E. Park, APL Mater. 3 (2015) 126105.

[~~45~~46] H. Yan, G. Manion Joseph, M. Yuan, F. P. García de Arquer, R. McKeown George, S. Beaupré, M. Leclerc, H. Sargent Edward, S. Seferos Dwight, Adv. Mater. 28 (2016) 6491.

Highlights

- Low-cost black phosphorus (BP) made from solution synthesis is integrated in organic solar cells (OSCs) via a simple solution process.
- An impressive fill factor (FF) of 74.2% and power conversion efficiency (PCE) of 10.5% were realized in the OSCs incorporating 10wt% of BP in the active layer of a benchmark material system, corresponding to a 20% PCE enhancement compared to the BP-free binary devices.
- The performance enhancement has been demonstrated in several photovoltaic material systems.
- BP's high hole carrier mobility facilitates better carrier extraction and suppression of the recombination, resulting in improved device characteristics.